

Study of the Effect of Load Torque on the Iron Losses of Permanent Magnet Motors by using Finite Element Analysis

Nguyen Gia Minh Thao^{*a)} Non-member, Nicolas Denis^{*} Non-member
Yenyi Wu^{*} Non-member, Shunya Odawara^{*} Member
Keisuke Fujisaki^{*} Senior Member

(Manuscript received April 13, 2018, revised Nov. 16, 2018)

The output torque of a three-phase interior permanent magnet synchronous motor (IPMSM) can be controlled within its allowable range using a pulse-width modulation (PWM) DC-AC inverter. In this paper, the effect of load torque on the iron losses of an IPMSM is studied by considering three different driving conditions, namely no-current, no-load, and load conditions. In order to perform a careful evaluation in the experiments, the motor is tested at various rotational speeds, namely 750 min^{-1} , 1500 min^{-1} , and 2250 min^{-1} ; the voltage modulation index of the PWM inverter and the load torque are also varied. The experimental results in all the test cases show that the iron losses of the motor vary when the excitation condition is varied among the no-current, no-load, and load cases. Furthermore, a three-dimensional (3D) finite element analysis (FEA) is performed for the main test case when the motor is operated at the rated speed of 750 min^{-1} for reference purpose. The harmonic components caused by the excitation inverter in the stator voltage, current, and magnetic flux density are found to be the main reasons for the increase in iron losses of the motor in the no-load and load conditions compared to the no-current condition; an increase in torque also causes a relatively significant increase in the iron losses.

Keywords: finite element analysis, interior permanent magnet synchronous motor, iron loss, PWM inverter, effect of load torque

1. Introduction

Since electrical motors are being more and more utilized for home appliances, industrial machine systems and automotive technologies, improving their efficiency is becoming crucial in order to lower the burden on electrical energy production. Due to the variation of magnetic flux, the iron losses occur in the motor magnetic cores. In an effort to decrease them, a lot of studies have been carried out to analyze the iron loss phenomena⁽¹⁾⁻⁽¹¹⁾.

Interior permanent magnet synchronous motors (IPMSM) are often driven by pulse-width modulation (PWM) inverters. The output voltages of PWM inverters have strong high harmonic components and therefore a high total harmonic distortion (THD), especially for two-level inverters⁽¹⁾. The PWM inverter output voltage supplied to wound soft-magnetic material cores or electrical motors tends to increase iron losses compared to the case of pure sinusoidal voltage supply⁽²⁾⁽³⁾. The impact of the PWM parameters, such as the carrier frequency⁽⁴⁾ or voltage modulation index⁽⁵⁾, on electrical motor iron losses has been studied. The relation between the number of inverter level and the motor iron losses has also been investigated in⁽⁶⁾.

Using the three-dimensional (3D) finite element analysis (FEA) to calculate the iron losses of a PWM inverter-fed

IPMSM, it has been found that the iron loss increase caused by PWM primarily concerns eddy current loss, with the worst impact on magnets⁽⁷⁾. Furthermore, an analytical model has been developed to evaluate the impact of the load on the rotor iron losses of a high-speed permanent magnet synchronous motor (PMSM)⁽⁸⁾; this research showed that the load can sensibly increase the rotor iron losses. Impacts of PWM voltage modulation index on motor iron losses in only the no-load condition were shown in⁽⁹⁾⁽¹⁰⁾.

Nevertheless, the impact of the load on motor iron losses has not been enough considered. The existing papers in⁽¹⁾⁻⁽¹¹⁾ only considered motor iron losses either in no-load condition or load condition, but they did not study and compare both the operational conditions in numerical analysis with 3D model and experiments. We found no paper that clearly deals with this problem in detail. The impact of the load can be estimated by comparing the load and no-load conditions, especially differences in voltage, current, magnetic flux density waveforms at different points in the motor core, characteristics of harmonic components, and iron losses. This is the key originality of our research.

In addition, manufacturers often provide characteristics of motor iron losses under the no-load condition only. However, let us note that the characteristics of motor iron losses in the no-load condition cannot be considered true and suitable for every load condition. In an electric vehicle (EV), the motors connected with wheels are operated in both the no-load and load conditions. The no-load condition can be considered as a special case with a very tiny load torque, while the

a) Correspondence to: Nguyen Gia Minh Thao. E-mail: ngmthao@toyota-ti.ac.jp

* Toyota Technological Institute
2-12-1, Hisakata, Tenpaku-ku, Nagoya, Aichi 468-8511, Japan

load condition is with many real operation modes of the EV, especially when the load torque or the increasing rate of the EV speed is large. Therefore, the iron loss characteristics of the IPMSM in no-load and load conditions should be examined and compared by 3D numerical analysis and various test cases to develop a high-efficient motor drive system utilized for the actual EV; this is the main usefulness of this study.

In this paper, three different driving conditions, namely no-current, no-load and load, are tested to evaluate detailed effects of the load on iron losses of the PWM inverter-fed IPMSM; the analyzed and measured values in the no-current condition are used for reference purpose only. In experiments, the motor is operated at different rotational speeds of 750 min^{-1} , 1500 min^{-1} and 2250 min^{-1} ; in addition, the PWM voltage modulation index is adjusted to various values of 0.25, 0.45, 0.67 and 0.9 for evaluation; the load torque is suitably set at $0.5 \text{ N}\cdot\text{m}$, or $0.67 \text{ N}\cdot\text{m}$, or $1 \text{ N}\cdot\text{m}$ to ensure a good operation for the motor system in each test case. Moreover, the 3D FEA in simulation is conducted to assess impact of the load on three different parts of the motor core (i.e. magnets, edge of rotor, and stator tooth) in the first test case. The magnetic flux density and eddy current losses are also analyzed by the 3D FEA.

The remaining of this paper is organized as follows. Section 2 briefly presents the IPMSM characteristics. Section 3 shows the experimental methodology with details on the different three driving conditions. Section 4 explains the 3D FEA and the numerical calculation of the iron losses. Section 5 gives the experimental and numerical analysis results in the first test case when the motor is operated at the rated speed of 750 min^{-1} . Three additional test cases in experiments when the motor is operated at the higher speeds are considered in Section 6. The conclusion and future work are presented in the last section.

2. Electrical Motor Characteristics

The electrical motor used in this paper is a three-phase IPMSM with concentrated windings; it has 8 poles and 12 stator slots. The quarter cross-section view and the related dimensions are illustrated in Fig. 1; besides, the stator tooth

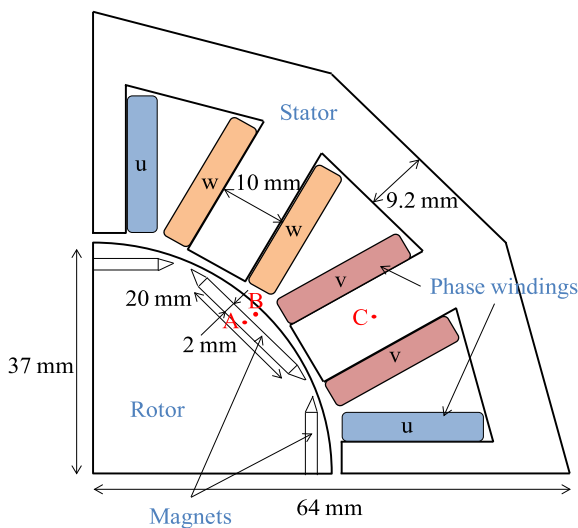


Fig. 1. Quarter cross-section view of the IPMSM

Table 1. Electrical characteristics of the IPMSM

Phase resistance R_s	0.498 Ω
d-axis inductance L_d	2.44 mH
q-axis inductance L_q	3.70 mH
Peak line to neutral back-EMF at 750 min^{-1}	20.1 V
Rated output power	400 W
Rated torque	1 N·m
Rated rotational speed	750 min^{-1}

and yoke have a similar thickness of 47 mm. In this figure, the radial magnetic flux density waveforms are obtained from the 3D FEA at three different points at the surface of the model; those are located on the magnet (point A), the edge of the rotor (point B) and the stator tooth (point C). The magnets are sintered NdFeB; the stator and rotor soft magnetic material is the non-oriented silicon steel 35H300. The main electrical characteristics of the motor are presented in Table 1, in which the phase resistance R_s is measured under DC condition. This motor is an experimental design prototype in our laboratory for research on direct motor drives used in future EVs.

3. Experimental Methodology

First, the motor is operated for warming-up purpose for ninety minutes. Then, from the time $t = 90$ minute to 120 minute, and from the time $t = 140$ minute to 180 minute, we perform seven measurements in total; each measurement has ninety samples and is collected for ten minutes. There are 630 data samples for all the measurement times of each experiment. For each operational condition (i.e. no-current, no-load, and load tests), we perform four independent times of experiment; each experiment is also conducted and checked carefully to obtain the reliable data. Last, the result is the average value of all the times of experiment.

3.1 No-current Test The experimental set-up of the no-current test is presented in Fig. 2. During this test, the IPMSM is rotated by an auxiliary brushless DC (BLDC) motor. The tested IPMSM armature windings are in open circuit so that no current flows. A torque meter is connected between the two motors in order to measure the mechanical output power of the BLDC motor P_{BLDC} , which is considered to be the sum of the IPMSM iron losses in no-current condition P_{i_noc} and its mechanical friction losses P_f as follows.

$$P_{BLDC} = \omega T_{BLDC} = P_{i_noc} + P_f \dots \dots \dots (1)$$

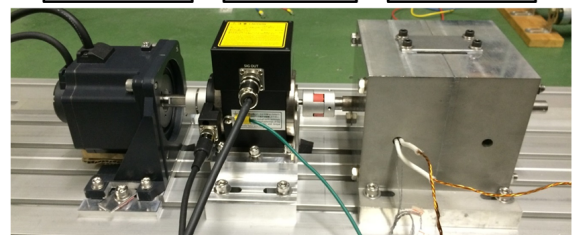
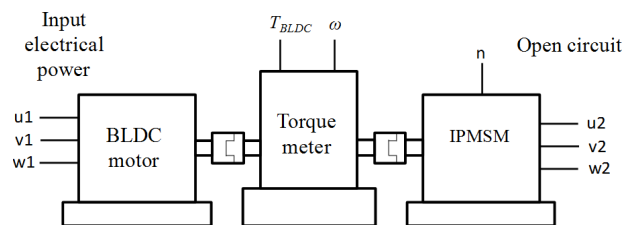


Fig. 2. Experimental set-up of the no-current test

Where ω is the measured speed in rad/s and T_{BLDC} is the measured torque in N·m. The iron losses $P_{i_{noc}}$ are considered to be the sum of the magnets, rotor and stator iron losses that are produced only by the rotating magnets. In order to estimate $P_{i_{noc}}$, P_f has to be measured by a preliminary test. This preliminary test consists in replacing the IPMSM rotor by a rotor with demagnetized permanent magnets and then performing the same test as in Fig. 2. Using demagnetized permanent magnets, no iron loss occurs in the IPMSM and the term $P_{i_{noc}}$ disappears in (1). The measured BLDC output power is then considered as an approximation of P_f . The torque meter is Onosokki TH-3104H, which accuracy is equal to ± 0.002 N·m and maximum measurable torque equal to 1 N·m.

Furthermore, in the no-load and load tests, an external encoder will be used for rotational speed feedback of the IPMSM to the PWM inverter control. Although the encoder has small mechanical resistance, the encoder mechanical loss can be estimated using a modified no-current test, in which an external encoder will be additionally connected to the right side of the IPMSM shaft in Fig. 2. In this modified no-current test, (1) is now rewritten as follows.

$$P_{BLDC_enc} = \omega T_{BLDC_enc} = P_{i_{noc}} + P_f + P_{enc} \dots \dots (2)$$

Where P_{BLDC_enc} is the measured total mechanical output power of the auxiliary BLDC motor and T_{BLDC_enc} is the measured torque in this modified no-current test. From (1) and (2), the encoder mechanical loss P_{enc} now can be computed as

$$P_{enc} = P_{BLDC_enc} - P_{BLDC} = \omega(T_{BLDC_enc} - T_{BLDC}) \dots \dots \dots (3)$$

For reference, the measured values of P_{enc} in this study are 0.1571 W, 0.3142 W, and 0.4712 W in cases when the motor is operated at speeds of 750 min^{-1} , 1500 min^{-1} , and 2250 min^{-1} , respectively. The consideration of encoder mechanical loss P_{enc} in evaluating motor iron losses in the load test and the experimental method used to measure P_{enc} are also the one of contributions of this paper as compared to other existing related research works.

3.2 No-load Test The experimental set-up of the no-load test is depicted in Fig. 3. The IPMSM is driven by a PWM inverter. A power analyzer is used to measure the IPMSM input active electrical power $P_{3\phi}$, phase rms currents I_u , I_v , I_w and the phase voltages. The power analyzer employed in this research is Yokogawa PX8000; it uses internal shunt resistances for the current measurement and has a sampling frequency of 100 MHz and a bandwidth of 20 MHz. Where P_{enc} is computed in (3), the total iron loss of the IPMSM under the no-load condition $P_{i_{nol}}$ is calculated as follows.

$$P_{i_{nol}} = P_{3\phi} - R_s(I_u^2 + I_v^2 + I_w^2) - P_f - P_{enc} \dots \dots \dots (4)$$

The PWM carrier signal is triangular-shaped with the default frequency of 1 kHz in test cases when the motor speed is 750 min^{-1} (Section 5) or 1500 min^{-1} (Subsections 6.1 and 6.2); the carrier frequency is only slightly changed to 2 kHz once the motor speed is 2250 min^{-1} (Subsection 6.3) for a

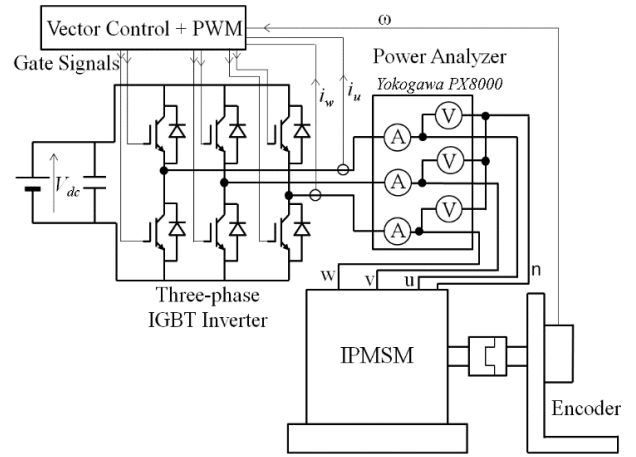


Fig. 3. Experimental set-up of the no-load test

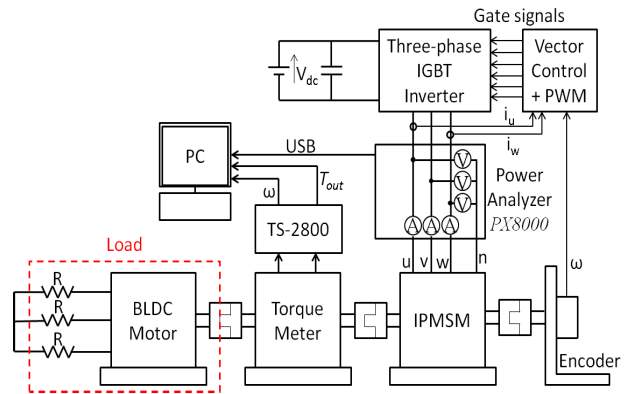


Fig. 4. Experimental set-up of the load test

good operation of the experimental motor system. The dead-time of the inverter is $3.5 \mu\text{s}$, and the d-axis current I_d is controlled to follow its reference value of 0 A. The default value of DC bus voltage V_{dc} is set to 180 V.

Only in a test case when the motor speed is 1500 min^{-1} in Subsection 6.2, V_{dc} is reduced from 180 V to 90 V to significantly increase the voltage modulation index in the PWM inverter for evaluation purpose.

3.3 Load Test The experimental set-up of the load test is illustrated in Fig. 4. The PWM inverter drive system and the IPMSM input power measurement method are identical to what is used during the no-load test. Contrary to the no-load test, a mechanical load composed of a BLDC motor and a resistance network is connected to the IPMSM rotor shaft. By adjusting the resistance network, the IPMSM output torque is close to 1 N·m at the rotational speed of 750 min^{-1} (Section 5) and 1500 min^{-1} (Subsection 6.1), or 0.5 N·m at the rotational speed of 1500 min^{-1} (Subsection 6.2), or 0.67 N·m at the rotational speed of 2250 min^{-1} (Subsection 6.3). A torque meter is placed between the IPMSM and the BLDC motor in order to measure the IPMSM output power T_{out} and the shaft rotational speed ω . The torque meter in use is Onosokki SS-020. It can measure a maximum torque of 2 N·m and its accuracy is equal to ± 0.004 N·m. The total iron loss of the IPMSM under the load condition $P_{i_{loa}}$ is calculated using the following equation

$$P_{i_{loa}} = P_{3\phi} - R_s(I_u^2 + I_v^2 + I_w^2) - P_f - P_{enc} - \omega T_{out} \dots \dots \dots (5)$$

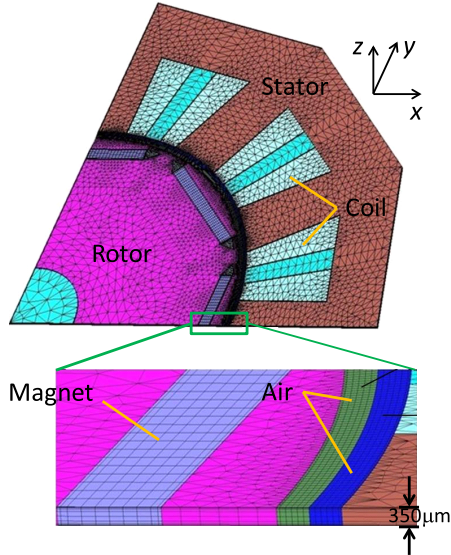


Fig. 5. 3D finite element model of the IPMSM

4. Finite Element Method for the Iron Loss Calculation

A 3D mesh model built with JMAG software is used for the FEA and is presented in Fig. 5. Only one quarter of the IPMSM axial cross-section is considered, and the axial length is equal to the steel sheet thickness of $350\ \mu\text{m}$. A time-stepping magnetic field analysis is performed using the 3D vector potential equation

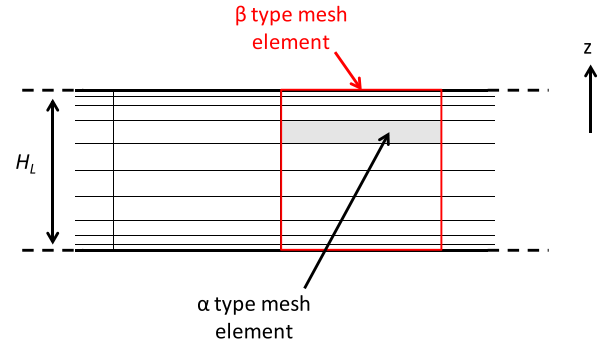
$$\nabla \times \left(\frac{1}{\mu} \nabla \times \vec{A} \right) = \vec{J}_0 - \sigma \left(\frac{\partial \vec{A}}{\partial t} + \nabla \Phi \right) + \frac{1}{\mu_0} \nabla \times \vec{M} \dots \dots \dots (6)$$

$$\nabla \cdot \left(\sigma \left(\frac{\partial \vec{A}}{\partial t} + \nabla \Phi \right) \right) = 0 \dots \dots \dots (7)$$

Where \vec{A} is the magnetic vector potential, Φ is the electric scalar potential, \vec{J}_0 is the stator phase current density, σ is the electrical conductivity of the material, μ is the magnetic permeability and \vec{M} is the PM magnetization. σ and μ depend on the considered material (electrical steel or magnet), and the magnetic permeability of the magnet is considered equal to that of the air μ_0 .

The stator phase current density is the input of the model. While it is equal to zero in the no-current condition, it is not zero in the no-load and load conditions. In the later cases, the current density obtained by measurement is used as the input to the model.

Since there are reflection symmetries, the periodic boundary conditions are applied at the edges of the model. In addition, the Dirichlet boundary condition is applied at the interlamination (air) surface boundaries, which means that the vector potential and the axial component of the magnetic flux density B_z are considered locally null in the vicinity of these surfaces. The assumption on the interlamination boundary condition might lead to inaccuracies but allows considering the lamination sheet individually. This has the advantage of considerably decreasing the computation time as compared to the case when the full axial length of the motor is considered in numerical simulation.


 Fig. 6. Introduction of fictional β mesh element for the calculation of the hysteresis losses

4.1 Calculation of the Hysteresis Losses The hysteresis losses are calculated using the Steinmetz approximation. Because the Steinmetz equations are usually used for two-dimensional (2D) models only, the following calculation procedure is used to adapt the equations. The magnetic flux density is first averaged over the axial direction. As an illustration, let α be the mesh element which composes the actual mesh of the 3D model and is defined by its radial, tangential and axial coordinates in the 3D space. Now let β be the element of a fictional mesh which groups the mesh elements in the axial direction as illustrated in Fig. 6.

This element is defined by its radial and tangential coordinates only and does not depend on the axial coordinate. Equations (6) and (7) are solved to obtain the radial, tangential, and axial components of the magnetic flux density in the mesh elements α . They are respectively noted $B_{r,\alpha}$, $B_{t,\alpha}$, and $B_{z,\alpha}$. Let (i,j,k) be the coordinate index of a given mesh element α , in which i represents the radial coordinate, j the tangential coordinate, and k the axial coordinate. The magnetic flux density of the β mesh element is the average of the magnetic flux density in each α mesh element inside the β mesh element.

For example, the radial component of the magnetic flux density in the mesh element β is

$$B_{r,\beta}(i, j) = \sum_{k=1}^{N_z} \frac{B_{r,\alpha}(i, j, k) h_k}{H_L} \dots \dots \dots (8)$$

where N_z is the mesh division in the axial direction ($N_z = 10$), h_k is the dimension of the mesh element α in the axial direction, and H_L is the lamination thickness. The same calculation applies for the tangential component $B_{t,\beta}$, but the axial component $B_{z,\beta}$ is supposed negligible and is not considered in the hysteresis loss calculation for matter of consistency with the 2D nature of the Steinmetz equations. After the above calculation, a fast Fourier transform (FFT) is then performed on the time-varying waveforms of the magnetic flux densities $B_{r,\beta}$ and $B_{t,\beta}$ in order to obtain the magnitude of the harmonic components $B_{r,\beta,n}$ and $B_{t,\beta,n}$. The hysteresis loss density in a given β mesh element is calculated by

$$W_{hys} = \sum_{n=1}^{N_h} K_{hys,n} (B_{t,\beta,n}^2 + B_{r,\beta,n}^2) f_n \dots \dots \dots (9)$$

where n is the harmonic order, N_h is the maximum harmonic order, f_n is the frequency of the n^{th} harmonic, and $K_{hys,n}$ is the

hysteresis loss coefficient derived from the material specific iron loss data, which depends on the frequency, as denoted by the subscript n .

4.2 Calculation of the Eddy Current Losses In each mesh element α and at each time-step of the simulation, the magnet, stator and rotor eddy-current density vector $\vec{J}_{e,\alpha}$ is calculated based on the electrical field. This field is itself derived from the electric scalar potential Φ . As expressed in (10), the calculation of the eddy-current loss density W_{ed} in a given α element is based on the integration of the eddy-current density through time considering the electrical conductivity σ .

$$W_{ed} = \frac{\kappa}{T_e} \sum_{t=1}^{N_t} \frac{|\vec{J}_{e,\alpha}(t)|^2}{\sigma} dt \dots \dots \dots (10)$$

where κ is the anomaly factor used as approximation to take the anomalous loss into account. Its value is 2 for the electrical steel used in the rotor and stator, and 1 for the magnets. T_e is the electrical period, N_t is the number of time-steps of the analysis, and dt is the time-step duration.

5. Experimental and Numerical Analysis Results in Case 1: With the rated motor speed of 750 min⁻¹

In this case, the motor is operated with a rotational speed of 750 min⁻¹, and the load torque is adjusted to 1 N·m in the load condition. The results of experimental results and numerical calculation are presented in Fig. 7. Differences between the numerical calculation and experimental results can be observed but stay small. Both numerical calculation and experiments show the largest iron losses for the load condition, closely followed by the no-load condition, while the lowest iron losses are obtained in no-current condition. Note that the detailed comparison between the no-load and load conditions is the key goal of this paper; the measured and analyzed values in the no-current mode are only used as reference values. Observing the FEA results, it can be seen that the hysteresis losses in the stator and rotor are almost equal in every working condition but there is a significant difference in the eddy current losses. Let us note that this is the main test case of this paper; the three additional test cases will be also performed in Section 6 for more detailed consideration and evaluation.

5.1 Analysis of the Phase Voltage The u phase to neutral voltage measured under the three conditions is depicted in Fig. 8. In the no-current condition, the rotation of the magnet is responsible for a varying magnetic flux in the stator, which induces a voltage (black curve) in the phase windings.

Contrary to the no-current condition, high frequencies appear in the phase voltage measured under the no-load and load conditions, due to the inverter switching operation. In order to observe the high-frequency harmonics, a discrete Fourier transformation (DFT) is performed and the magnitude of the voltage harmonics are presented in Fig. 9. Only the fundamental, 5th and 7th harmonics appear in the no-current condition. High order harmonics due to PWM appear only in the no-load and load conditions. Moreover, it can be noticed that both the PWM high order harmonics and the

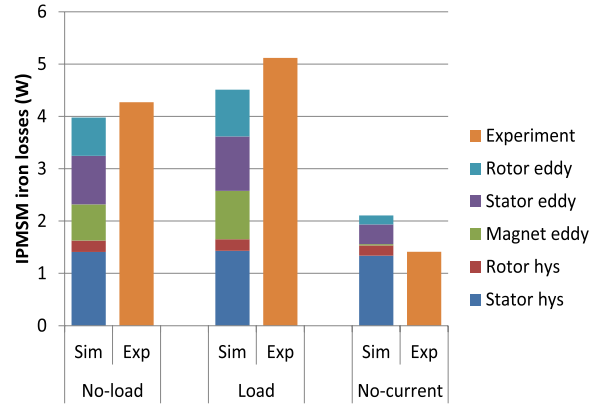


Fig. 7. Experiment and numerical calculation results comparison for no-current, no-load and load tests, Case 1

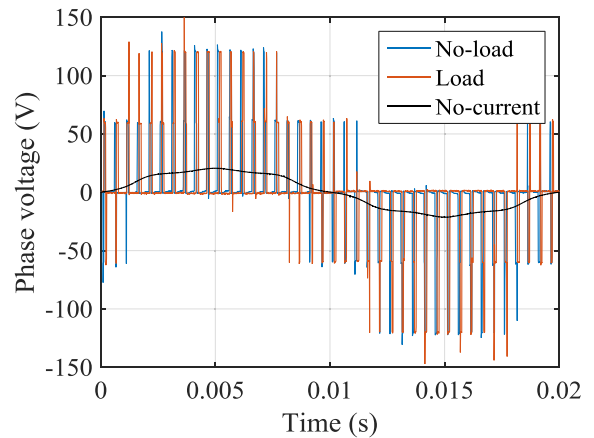


Fig. 8. Phase voltage waveform under no-load, load and no-current conditions, Case 1

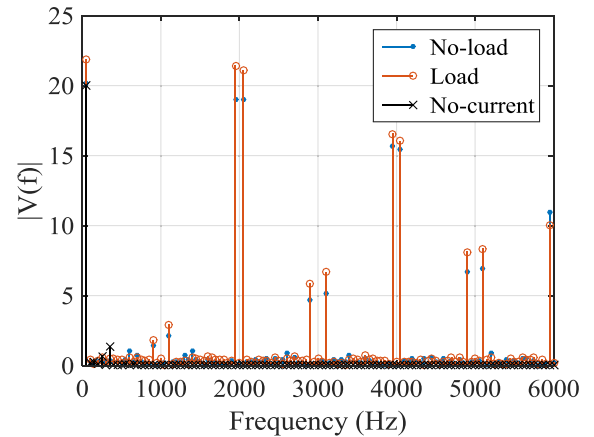


Fig. 9. DFT of phase voltage waveform, Case 1

fundamental value are higher in the load condition as compared to the no-load condition. This can be explained by the fact that during the load condition, the IPMSM fundamental current is obviously higher than the one in the no-load condition in order to output a higher torque.

Because of the motor phase impedance, the higher fundamental current implies the higher fundamental voltage. The rms value of the fundamental phase voltage can be approximated by the following equation

$$V_{f,rms} = m \frac{V_{dc}}{2\sqrt{2}} \dots \dots \dots (11)$$

where m is the PWM voltage modulation index.

Since V_{dc} is fixed at 180 V in this case, the vector control adjusts m to control the IPMSM fundamental phase voltage. Accordingly, m is equal to 0.241 in the no-load condition and 0.266 in the load condition. The increase of the voltage modulation index not only efficiently increases the fundamental voltage but also has the adverse effect of increasing the amplitudes of the PWM high order harmonics⁽⁹⁾. In this study, the effect of the higher values for the voltage modulation index on the iron losses of the motor will be presented and examined in Section 6.

5.2 Analysis of the Phase Current The phase currents measured under no-load and load conditions are illustrated in Fig. 10. The amplitudes of the current harmonics obtained by DFT are described in Fig. 11. The operation in the load condition clearly increases the fundamental current, but the high order harmonics due to the PWM also have larger amplitudes. This is the direct consequence of the larger voltage at high-order harmonics in the load condition. The phase current is responsible for magnetomotive forces originating from the stator windings and having an effect on the magnetic flux density in the stator, rotor and magnets. The actual value of the d-axis current I_d slightly fluctuates around the reference value $I_d^{ref} = 0$ A; and its measured fluctuation range

is $(-0.405$ A, 0.405 A). The measured value of q-axis phase current I_q is 3.349 A. The armature current phase angle φ_i can be computed according to (12), and its value is small in the range of $(-0.12$ rad, 0.12 rad).

$$\varphi_i = \tan^{-1} \left(\frac{I_d}{I_q} \right) \dots \dots \dots (12)$$

The next subsection presents a detailed analysis of the magnetic flux density in the three operating conditions by use of the 3D FEA numerical calculation results. As depicted in Figs. 9 and 11, the magnitudes of harmonic components in the voltage and current waveforms of IPMSM increase pretty significantly in the load condition as compared to the ones in the no-load condition.

5.3 Analysis of the Magnetic Flux Density Using the FEA, the magnetic flux density waveform can be observed at any point of the motor model. The radial magnetic flux density waveform has been obtained from the FEA at three different points located at the surface of the model. These points are located on the magnet (point A), the edge of rotor (point B), and the stator tooth (point C), as described in Fig. 1. The magnetic flux density waveforms at the above three points are illustrated in Fig. 12. The fundamental frequency of the waveform is three times the electrical frequency. This is due to the slot effect (the IPMSM has three slots per pole pair). Moreover, the magnetic flux density waveform under the load condition has more ripple than ones under the no-current and no-load conditions.

This is also observed in the DFT illustrated in Fig. 13 in which high order harmonics appear only for no-load and load conditions. This is the effect of the PWM high order harmonics in the phase current observed back in Figs. 10 and 11. It can also be seen that because the fundamental current under no-load condition is almost null, the fundamental of the magnetic flux density is almost the same between no-current and no-load conditions. However, both the fundamental and the high order harmonics of the magnetic flux density are larger under the load condition than under the no-load condition. This is thought to be due to the increase in both fundamental and high order harmonic components of the current under the load condition as compared to the no-load condition, which are observed and commented in the previous subsection.

In order to more clearly quantify the effect of the load on the magnetic flux density, the harmonic content of the waveforms is calculated. The harmonic content of the magnetic flux density in a given harmonic order range $[N_1; N_2]$ is given by

$$B_{r,\alpha,harm} = \sqrt{\sum_{n=N_1}^{N_2} B_{r,\alpha,n}^2} \dots \dots \dots (13)$$

Table 2 gives the amplitude of fundamental and the complete harmonic content excluding the fundamental ($N_1 = 2$, $N_2 = N_h$) of the radial magnetic flux density at the points A, B and C for both no-load and load conditions. In the magnets, rotor and stator, both the harmonic content and the fundamental are higher in load condition. Moreover, it can be seen that the strongest increase rate occurs in the magnets, followed by the rotor and finally the stator. In particular, the increase of fundamental in the rotor and stator is almost null. Since

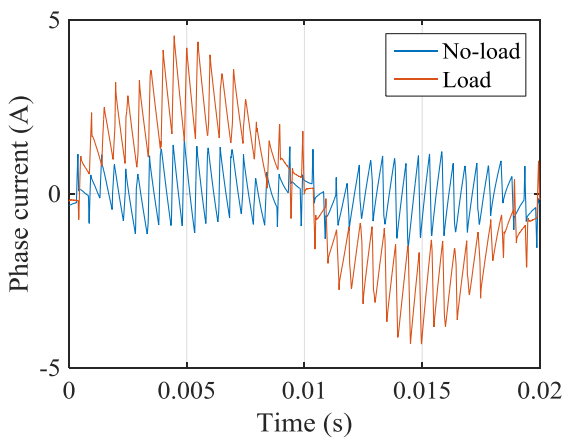


Fig. 10. Phase current waveform under no-load and load conditions, Case 1

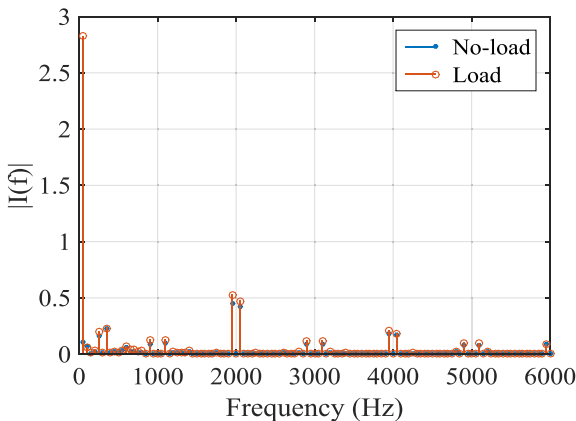


Fig. 11. DFT of phase current waveform, Case 1

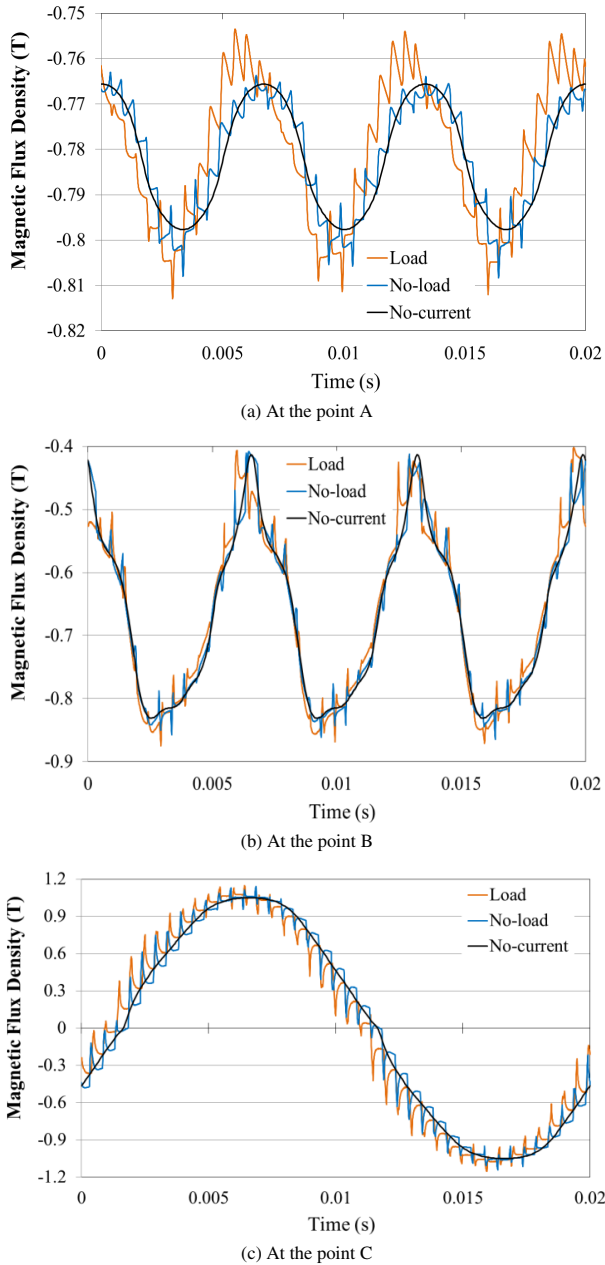


Fig. 12. Radial magnetic flux density in three points A, B, and C under no-current, no-load, and load conditions, *Case 1*

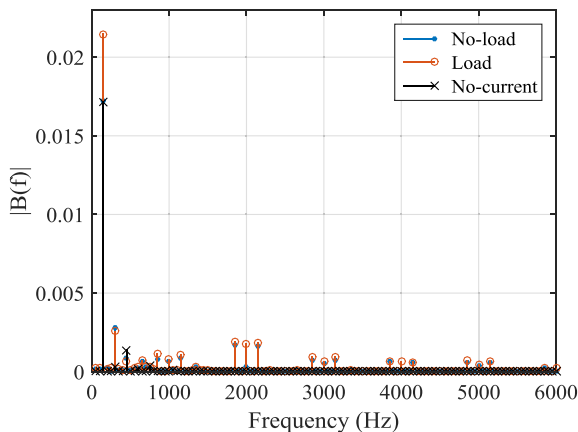


Fig. 13. DFT of radial magnetic flux density waveform in the magnet, *Case 1*

Table 2. Comparison of fundamental and harmonic content of radial magnetic flux density in no-load and load conditions in *Case 1*

		No-load	Load	Increase rate
Magnet (point A)	Fundamental (150 Hz)	0.0172 T	0.0215 T	24.82 %
	Harmonic content	0.0046 T	0.0052 T	14.31 %
Rotor (point B)	Fundamental (150 Hz)	0.1802 T	0.1844 T	2.31 %
	Harmonic content	0.0400 T	0.0440 T	10.06 %
Stator (point C)	Fundamental (50 Hz)	1.0727 T	1.0785 T	0.54 %
	Harmonic content	0.0973 T	0.1050 T	7.94 %

the eddy current losses basically increase with the square of the magnetic flux frequency, it is thought that the increase of high order harmonic content in the load condition is the main cause of the stronger eddy current losses observed in the magnets, rotor and stator as depicted in Figs. 7 and 14. Moreover, the eddy current loss density in load condition is fairly much larger than the one in no-load condition as presented in Fig. 14.

However, the hysteresis losses see almost no change, which means that the increase reported in Table 2 is too small to affect them. Moreover, it is thought that the large increase rate, combined with the fact that the magnet is not segmented and then offers a large radial area, can explained the fact that the eddy current losses increase substantially in the magnets.

It is noted that the content presented and discussed in this section, including noticeable differences in the obtained results between no-load and load operational conditions shown in Figs. 7 to 14 and Table 2, is one of the key originalities and contributions of this paper as compared to other existing related works.

6. Experimental Results in Three Additional Test Cases

6.1 Case 2: With Motor Speed of 1500 min^{-1} and Medium Voltage Modulation Index of 0.45 In this case, the motor is operated with a rotational speed of 1500 min^{-1} , and the DC bus voltage V_{dc} is fixed at 180 V; the load torque is adjusted to 1 N·m in the load condition. All the no-current, no-load and load conditions are considered and conducted in experiments; the experimental results are shown in Fig. 15. In detail, the total iron losses of the IPMSM in the no-current, no-load, and load tests are 5.341 W, 12.084 W, and 14.034 W, respectively. As compared to the no-current test, the total iron loss of the motor significantly increases 226.25% and 262.76% in the no-load and load tests, respectively. Furthermore, the total iron loss of the motor in the load condition is larger 16.16% than the one in the no-load condition.

The main goal of this test is to compare with the obtained results in *Case 1* (see Fig. 7) when the motor speed is increased from 750 min^{-1} to 1500 min^{-1} . As a result, once the motor speed is increased, the total motor iron loss increases, and the total iron loss in load condition is still larger than the

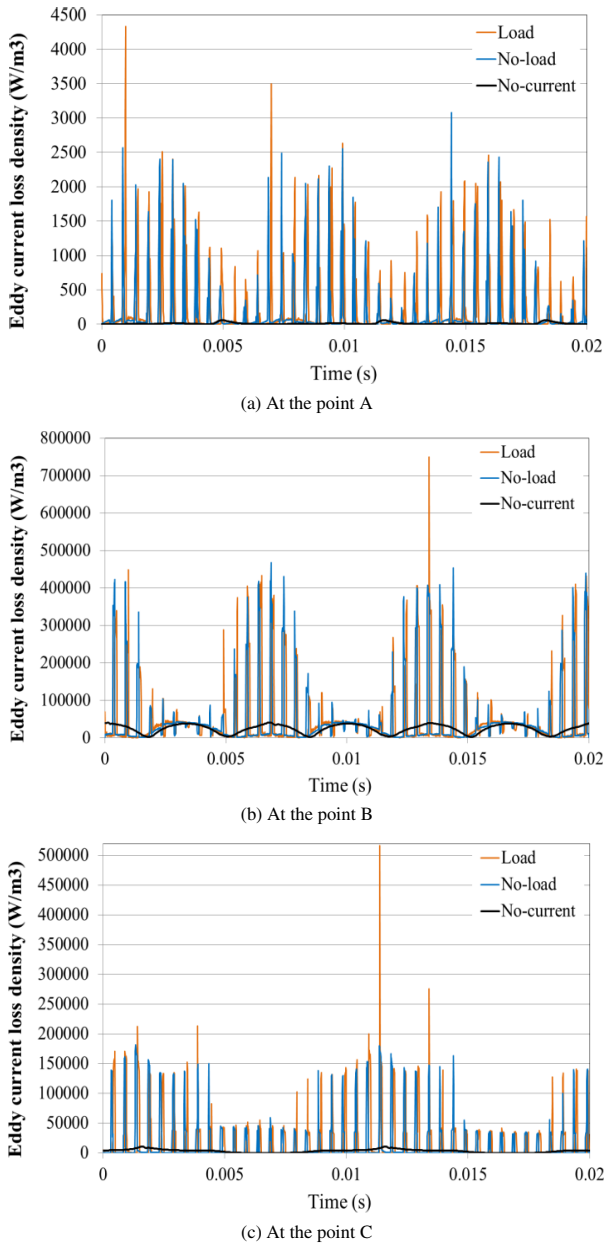


Fig. 14. Eddy current loss density at the three points A, B, and C under no-current, no-load, and load conditions, *Case 1*

one in no-load mode.

The PWM voltage modulation indexes m in the no-load and load conditions are 0.445 and 0.46, respectively. The actual value of the d-axis current I_d slightly fluctuates around the reference value of 0 A; and its measured fluctuation range is $(-0.5 \text{ A}, 0.5 \text{ A})$. The measured value of q-axis phase current I_q is 3.37 A. According to (12), the actual armature current phase angle φ_i has a small value in the range of $(-0.147 \text{ rad}, 0.147 \text{ rad})$.

6.2 Case 3: With Motor Speed of 1500 min^{-1} and High Voltage Modulation Index of 0.9 In this case, the motor is operated with a rotational speed of 1500 min^{-1} , and the DC bus voltage V_{dc} is reduced from 180 V to be fixed at 90 V. For a stable operation of the experimental motor system, the load torque is reduced to 0.5 N·m in the load condition. All the no-current, no-load and load conditions are

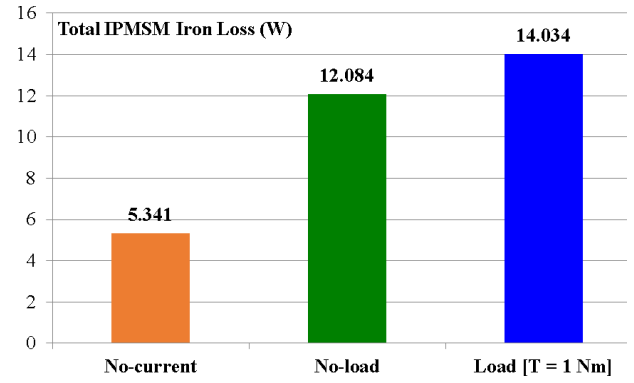


Fig. 15. Experimental results under no-current, no-load and load tests, *Case 2*

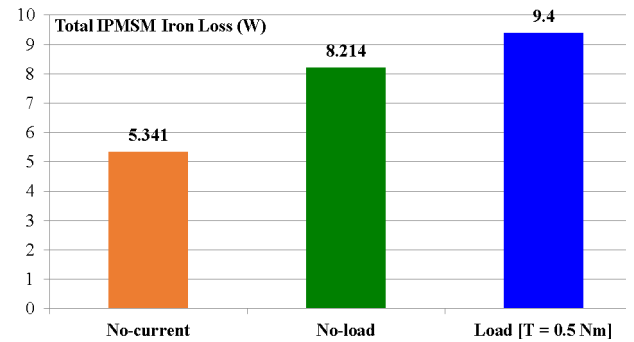


Fig. 16. Experimental results under no-current, no-load and load tests, *Case 3*

considered and performed in experiments; the experimental results are depicted in Fig. 16. In detail, the total iron losses of the IPMSM in the no-current, no-load, and load tests are 5.341 W, 8.214 W, and 9.4 W, respectively. As compared to the no-current test, the total iron loss of the motor increases 153.79% and 176% in the no-load and load tests, respectively. Besides, the total iron loss of the motor in the load condition is larger 14.44% than the one in the no-load condition. The PWM voltage modulation indexes m in the no-load and load tests are 0.891 and 0.905, respectively.

As compared to the experimental results in *Case 2* (see Fig. 15), the total iron losses of the motor are relatively considerably reduced from 12.084 W to 8.214 W in the no-load test, and from 14.034 W to 9.4 W in the load test. The key reason here is the substantial increase of the PWM voltage modulation index from 0.445–0.46 in *Case 2* to 0.891–0.905, while the load torque value was chosen as 0.5 N·m in this case to ensure a stable operation of the experimental motor system. Furthermore, we see that once the PWM modulation index is with a high value of 0.9 under the fixed rotational speed mode, the total iron loss of motor in load mode is still fairly much larger than the one in no-load mode.

The actual value of the d-axis current I_d slightly oscillates around the reference value of 0 A, and its measured fluctuation range is $(-0.5 \text{ A}, 0.5 \text{ A})$. The measured value of q-axis phase current I_q is 1.79 A. According to (12), the armature current phase angle φ_i can be estimated, and its actual value varies in the range of $(-0.272 \text{ rad}, 0.272 \text{ rad})$.

6.3 Case 4: With Motor Speed of 2250 min^{-1} and Pretty High Voltage Modulation Index of 0.67 In this case, the motor is operated with a rotational speed of

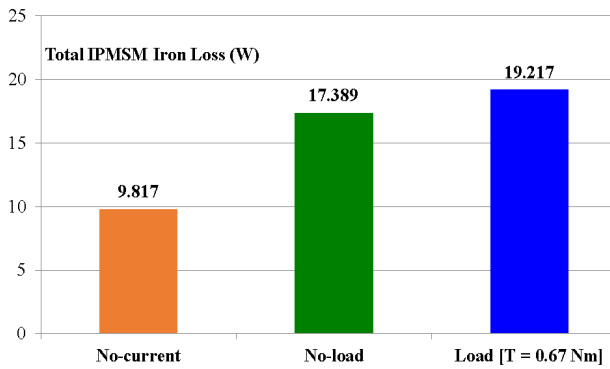


Fig. 17. Experimental results under no-current, no-load and load tests, *Case 4*

2250 min^{-1} , and the DC bus voltage V_{dc} is fixed at 180 V. For a good operation of the experimental motor system, the PWM carrier frequency is changed from 1 kHz to 2 kHz. The value of the resistor network connected to the BLDC motor (see Fig. 4) is kept same as the value set in *Case 3*. Because the motor speed is increased from 1500 min^{-1} to 2250 min^{-1} in this test case, the load torque is now measured as 0.67 N·m in the load condition.

All the no-current, no-load and load conditions are considered and conducted in experiments; the experimental results are described in Fig. 17. In detail, the iron losses of the IPMSM in the no-current, no-load, and load tests are 9.817 W, 17.389 W, and 19.217 W, respectively. As compared to the no-current test, the total iron loss of the motor increases noticeably 177.13% and 195.75% in the no-load and load tests, respectively. In addition, the total iron loss of the motor in the load condition is larger 10.51% than the one in the no-load condition.

The PWM voltage modulation indexes m in the no-load and load tests are calculated as 0.663 and 0.677, respectively. As compared to *Case 3*, although the PWM carrier frequency need be slightly increased from 1 kHz to 2 kHz for a stable operation of the motor in experiment, the iron losses of the motor in this case are large due to the remarkable increase of motor speed from 1500 min^{-1} to 2250 min^{-1} . The main aim of this test case is to validate that the total iron loss of motor in load condition is always larger than the one in no-load condition, even when the motor is operated with a high speed of 2250 min^{-1} and a pretty-high voltage modulation index of 0.67. The actual value of d-axis current I_d alters around the reference value of 0 A, and its measured fluctuation range is (-0.57 A, 0.57 A). The measured value of q-axis current I_q is 2.39 A. As given by (12), the armature current phase angle φ_i can be calculated, and its actual value is relatively small in the range of (-0.234 rad, 0.234 rad).

7. Conclusion

The experimental results demonstrated that, in the no-load test, lots of harmonic components produced by the PWM inverter on the IPMSM magnetic flux density increase iron losses of the motor noticeably as compared to the no-current test. Furthermore, when the motor is operated in the load condition, since the magnitudes of harmonic components on the IPMSM magnetic flux density are noticeably increased as compared to the ones in the no-load condition, the total

iron loss of the motor increases relatively much, especially in the operational case with high load torque. The four different test cases in experiments with changes in the motor rotational speed, DC bus voltage, PWM voltage modulation index and load torque were conducted to extensively evaluate the effect of the load on the total iron loss of the motor. In general, it can be observed and concluded that if the rotational speed of the motor is increased or the load torque is increased, the total iron loss of the motor will increase. Besides, the actual value of the PWM voltage modulation index m heavily depends on the motor rotational speed and the DC bus voltage as described in (11) and the four experimental cases. Once the motor speed is fixed, if the voltage modulation index m is increased by decreasing the DC bus voltage, the total iron loss of the motor will decrease in both the no-load and load operational conditions, and vice versa.

In addition, in the first test case, the 3D FEA showed that the magnet eddy current losses are substantially impacted by a load torque increase in the load condition as compared to the no-load condition. It is clarified that the relation between the IPMSM iron losses and its load is caused by the higher PWM modulation index that is needed to increase the torque, which in turn increase the high order harmonics in the magnetic flux density.

In future work, the impact of the load on iron losses of the IPMSM under high rotational speeds with the flux weakening control technique, where the PWM voltage modulation index can be nearly equal to 1.0, will be investigated carefully. The eddy current distribution in the IPMSM using the 3D FEA will be also considered in detail. Moreover, a new control method with the changeable reference value for the d-axis armature current will be developed and implemented in an experimental IPMSM system.

Acknowledgment

This work was supported in part by the Ministry of Education, Culture, Sports, Science and Technology program, Japan, for private universities.

References

- (1) J.I. Leon, L.G. Franquelo, E. Galvan, M.M. Prats, and J.M. Carrasco: "Generalized analytical approach of the calculation of the harmonic effects of single phase multilevel PWM inverters", Proc. of 30th Annual Conference on the IEEE Ind. Electron. Soc., Busan, Korea, pp.1658–1663 (2004)
- (2) A. Boglietti, P. Ferraris, M. Lazzari, and F. Profumo: "Iron losses in magnetic materials with six-step and pwm inverter supply", IEEE Trans. on Magnetics, Vol.27, No.6, pp.5334–5336 (1991)
- (3) A. Boglietti, P. Ferraris, M. Lazzari, and M. Pastorelli: "Influence of the inverter characteristics on the iron losses in PWM inverter-fed induction motors", IEEE Trans. on Industry Applications, Vol.32, No.5, pp.1190–1194 (1996)
- (4) N. Denis, S. Odawara, and K. Fujisaki: "Attempt to evaluate the building factor of a stator core in inverter-fed permanent magnet synchronous motor", IEEE Trans. on Industrial Electronics, Vol.64, No.3, pp.2424–2432 (2017)
- (5) E. Maruyama, S. Sumita, and A. Nakahara: "Evaluation of increasing rates in eddy-current loss of the motor due to carrier frequency", Proc. of Int. Conf. on Electrical Machines, Berlin, Germany, pp.1153–1157 (2014)
- (6) L. Masisi, M. Ibrahim, J. Wanjiku, A.M. Aljehaimi, and P. Pillay: "The effect of two- and three-level inverters on the core loss of a synchronous reluctance machine (SynRM)", IEEE Trans. on Industry Applications, Vol.52, No.5, pp.3805–3813 (2016)
- (7) K. Yamazaki and A. Abe: "Loss investigation of interior permanent-magnet motors considering carrier harmonics and magnet eddy currents", IEEE Trans. on Industry Applications, Vol.45, No.2, pp.659–665 (2009)

- (8) H.-W. Cho, H.-K. Sung, J.-Y. Choi, D.-J. You, J.-H. Park, S.-M. Jang, and S.-H. Lee: "Analytical calculation of rotor losses in high-speed permanent magnet synchronous motor at different load conditions", *Journal of Applied Physics*, Vol.103, paper ID: 07F129 (2008)
- (9) N. Denis, Y. Wu, and K. Fujisaki: "Impact of the Inverter DC Bus Voltage on the Iron Losses of a Permanent Magnet Synchronous Motor at Constant Speed", *IEEE J. of Industry Applications*, Vol.6, No.6, pp.346–352 (2017)
- (10) A. Boglietti, P. Ferraris, M. Lazzari, and F. Profumo: "Effects of Different Modulation Index on the Iron Losses in Soft Magnetic Materials Supplied by PWM Inverter", *IEEE Trans. on Magnetics*, Vol.29, No.6, pp.3234–3236 (1993)
- (11) V. Ruuskanen, J. Nerg, M. Rilla, and J. Pyrhönen: "Iron Loss Analysis of the Permanent-Magnet Synchronous Machine Based on Finite-Element Analysis Over the Electrical Vehicle Drive Cycle", *IEEE Trans. on Industrial Electronics*, Vol.63, No.7, pp.4129–4136 (2016)

Nguyen Gia Minh Thao (Non-member) obtained B.Eng. (honors)



and M.Eng. (research) degrees in Electrical and Electronics Engineering from Ho Chi Minh City University of Technology (HCMUT), Vietnam, in March 2009 and April 2011, respectively. He obtained a Dr.Eng. degree in Electrical Engineering from Waseda University, Japan, in September 2015. In April 2009, he became a probationary Lecturer in the Faculty of Electrical and Electronics Engineering at HCMUT, where he has been a Lecturer since January 2012. He was a Postdoctoral Research Associate at Waseda University, Japan from November 2015 to October 2017. He is currently a Postdoctoral Fellow at the Research Center for Smart Vehicles and Electromagnetic Energy System Laboratory, Toyota Technological Institute, Japan from November 2017. His research interests include intelligent control, advanced control methods, power electronics, electric motor drives, motor losses evaluation, renewable energy systems, and energy network optimization. He is a member of the Institute of Electrical and Electronics Engineers (IEEE) and the Asian Control Association (ACA).

Nicolas Denis (Non-member) was born in France in 1987. He received the M.Eng. degree and the French Engineer Diploma degree in electrical engineering from the École Nationale Supérieure d'Électricité et de Mécanique de Nancy, Nancy, France, in 2010, and the Dr.Eng. degree in electrical engineering from Sherbrooke University, Sherbrooke, QC, Canada, in 2014. He was a Postdoctoral Fellow and Commissioned Scientist in the Toyota Technological Institute, Nagoya, Japan, from 2014 to 2017, in which he worked on electrical motors iron losses and application of efficient magnetic materials for electrical motors. He is currently engineer at Challengery Inc., Tokyo, Japan.



Yenyi Wu (Non-member) was born in Taichung, Taiwan in 1992. She received the B.S. degree in electronic engineering from National Kaohsiung Normal University, Kaohsiung, Taiwan, in 2014. She received the M.S. degree at National Chung Hsing University, Taiwan, and the double degree program between the Toyota Technological Institute, Japan, and National Chung Hsing University. Her research interests include Radio-Frequency integrated circuit design and the loss property of the iron core of the electrical motor.



Shunya Odawara (Member) was born in March 13, 1987. He received B. of Eng., M.Eng., and Dr.Eng. Degrees from Saga University, Saga, Japan, in 2009, 2010, and 2013, respectively. From 2013, he was in Toyota Technological Institute, Aichi, Japan as postdoctoral researcher. Now he is in Kitami Institute of Technology, Hokkaido, Japan as research associate from 2017. His current research theme is loss characteristics evaluation by inverter excitation taking account of magnetic property and semiconductor property.



Keisuke Fujisaki (Member) received the B.Eng., M.Eng., and Dr.Eng. degrees in electronics engineering from the Faculty of Engineering, The University of Tokyo, Tokyo, Japan, in 1981, 1983, and 1986, respectively. From 1986 to 1991, he conducted research on electromagnetic force applications to steel-making plants at the Ohita Works, Nippon Steel Corporation. From 1991 to 2010, he was a chief researcher in the Technical Development Bureau, Nippon Steel Corporation, Futtsu, Japan. Since 2010, he was a professor of Toyota Technological Institute. His current scientific interests are magnetic multi-scale, electromagnetic multi-physics, high efficient motor drive system, electrical motor, and power electronics. In 2002–2003, he was a Visiting Professor at Ohita University. In 2003–2009, he was a Visiting Professor at Tohoku University. Dr. Fujisaki received the Outstanding Prize Paper Award at the Metal Industry Committee sessions of the 2002 IEEE Industry Applications Society Annual Meeting.

